Supplementary Materials

Analyzing the Suitability of Remotely Sensed ET for Calibrating a Watershed Model of a Mediterranean Montane Forest

Steven M. Jepsen[1], Thomas C. Harmon[1], Bin Guan[2, 3]

1. University of California Merced, Department of Civil & Environmental Engineering and Environmental Systems Graduate Program, 5200 N. Lake Road, Merced, CA 95343, USA

2. Joint Institute for Regional Earth System Science and Engineering, University of California, Los Angeles, 607 Charles E. Young Drive East, Los Angeles, CA 90095, USA

3. Jet Propulsion Laboratory, California Institute of Technology, 4800 Oak Grove Drive, Pasadena, CA 91109, USA

S1. Construction of base watershed model in ArcSWAT

This section describes inputs and settings of the "base model" constructed in ArcSWAT 2012. Spatial datasets for elevation, soil, land use, and weather forcings are listed in supplement Table S1. The weather forcings were daily precipitation, minimum and maximum air temperature, relative humidity, downward solar radiation, and wind speed. Relative humidity was computed using dewpoint temperature, minimum air temperature, and maximum air temperature from the PRISM AN81d product (Daly et al., 2008, 2015; PRISM Climate Data) with the equation for saturation vapor pressure in Murray (1967). Downward solar radiation and wind speed were obtained from the GridMET product (Abatzoglou, 2013; Climatology Lab). Each subbasin of the SWAT model (Figure 1) was forced with a separate set of weather variables. These subbasin weather variables were obtained by downsampling the original 2.5-arcminute weather datasets by a factor of 16 (to ~250-m resolution), masking the downsampled weather data to each subbasin, and then calculating daily averages of the masked data. This was done in Python 3.7 with the packages rasterio, fiona, and shapely. The reference elevation for each set of subbasin weather forcings (i.e., the "gage" elevation) was set to the mean elevation of the corresponding subbasin.

The "critical source area," which defines the minimum drainage area required to form the origin of a stream, was set to 5000 ha producing a total of 47 subbasins (Figure 1). Three slope classes were defined at uniformly spaced percentile ranges (tertiles) of the slope distribution in the watershed digital elevation model (DEM). These slope classes were 0–14.3°, 14.3–26.1°, and greater than 26.1°. We selected the option to use multiple Hydrologic Response Units (HRUs) per subbasin, and set the associated "threshold areas" to 20% for land use, 10% for soil type, and 20% for slope class as suggested by Winchell et al. (2013). These settings for critical source area and threshold area produced a total of 444 HRUs in the SWAT model.

Five equal-area elevation bands per subbasin were defined based on uniformly spaced percentile ranges (quintiles) of the elevation distribution in the watershed DEM. This was done for each subbasin by first solving for elevations separating the five quintiles of the elevation distribution and then evaluating area-weighted mean elevations in each quintile. Computations for this were performed in Python 3.7 and resulting values entered manually into ArcSWAT.

Parameter values listed in Table S2 were manually entered into the graphic user interface of ArcSWAT.

S2. Watershed model initialization with LAI and biomass of mature forest

The HRUs of the base model from ArcSWAT had been configured with default "scheduled management operations" consisting of yearly "planting" and "harvest/kill" operations of the land cover to emulate cropping operations (Arnold et al., 2012 a). Using a series of Python 3.7 scripts, we replaced these scheduled management operations with continous growth conditions of a mature forest. To make this change, we first deleted the lines at the end of the SWAT input *.mgt files defining the yearly planting and harvest/kill operations. We then set values of five parameters in the "Initial Plant Growth Parameters" section near the beginning of the SWAT input *.mgt files, as follows. The first parameter, IGRO, is the land cover status code. We set IGRO to 1 to simulate a land cover growing at the beginning of a simulation. The second parameter, PLANT_ID, is the HRU land cover identification number. We set PLANT_ID to the value queried from the PLANT_ID field of the mgt2 table of the ArcSWAT project database (p. 386 in Winchell et al., 2013). We applied this query to an SQLite version of the ArcSWAT project database, originally provided as a Microsoft Access file in ArcSWAT, using the Python sqlite3 module. The third parameter, PHU_PLT, is the total number of heat units or growing degree days needed to bring a plant to maturity. We set PHU_PLT to the value queried from the HEATUNITS field of the mgt2 table of the ArcSWAT project database (SQLite version) (p. 386 in Winchell et al., 2013). The fourth and fifth parameters are LAI_INIT, initial leaf area index (LAI), and BIO_INIT, initial dry weight biomass (kg/ha). We set these equal to the final monthly outputs from a spin-up simulation of the base model to steady state conditions. This spin-up consisted of a SWAT simulation of the base model forced by dynamic steady-state weather conditions, consisting of daily averages of weather data from PRISM and GridMET during 2000–2019 (supplement Table S1), until LAI and biomass reached equilibrium. After some experimentation (supplement Figure S5), we decided to apply 30 years of steady state spin-up in order to bring LAI and biomass to approximate equilibrium.

After replacing the scheduled management operations in each HRU with continous growth conditions of a mature forest, as described above, we modified some of the SWAT biophysical parameters of the land covers to more closely reflect the forested conditions of the upper Kings River watershed (see supplement Table S3). After doing this, the SWAT model was referred to as the "plant spin-up model."

S3. Sensitivity analysis of influential watershed model parameters

We conducted a global sensitivity analysis to identify the most influential SWAT parameters to subsequently estimate via calibration. The most influential parameters were defined to be the set of parameters accounting for 99% of total modeled variance in calibration objective, defined to be the Kling-Gupta efficiency (KGE) (Gupta et al., 2009) of monthly streamflow. For the sensitivity analysis, we used the Sobol method which decomposes the total variance of the model objective into contributions from individual parameters (Saltelli et al., 2000). For this, we used the Python SALib package (Herman and Usher, 2017) for parameter sampling and sensitivity analysis, and the run batch file of the SWAT-CUP package with parallel processing license for carrying out the necessary SWAT simulations (Abbaspour et al., 2007; Yang et al., 2008; Rouholahnejad et al., 2012).

The first step in the sensitivity analysis was to select a set of possibly influential SWAT parameters and their ranges to be sampled in the Sobol method. Using the literature, known controls on evapotranspiration, and previous experience in the neighboring upper San Joaquin River (Jepsen et al., 2018), we selected 26 SWAT model parameters and ranges over which to sample them (Table S4). For the response function of the sensitivity analysis, as well as the objective function of calibration (section S4), we eventually selected the Kling-Gupta efficiency (KGE) (Gupta et al., 2009) of monthly modeled streamflow at the watershed outlet. This selection was made after first trying the Nash-Sutcliffe efficiency (NSE) (Nash and Sutcliffe, 1970) for sensitivity analysis response and calibration objective. However, this objective function for calibration resulted in unacceptably high values of model percent streamflow bias (PBIAS) ($\geq$ 15%) (Moriasi et al., 2007), even though NSE-values were good ($\geq$ 0.9).

The required number of SWAT simulations for the Sobol sensitivity analysis, which we configured to include first-order but not second-order interaction effects, is given by $N*(D + 2)$ where N is the sample size and D is the number of parameters, equal to 26. We used a sample size (N) of 1000 because it produced a 95% confidence interval equal to approximately 10% of the leading total-order (sensitivity) index, as suggested by Herman and Usher (2017). These settings required a total of 1000*(26 + 2) = 28,000 SWAT simulations. These simulations took approximately 84 hours to completele on a 3.4 GHz Windows 7 PC running 6 processes in parallel.

The results of the sensitivity analysis sorted by total order (TO) index are shown in Table S5. When all TO indices are normalized such that they sum to unity, the TO index of a particular parameter gives that parameter's fractional contribution to the total modeled KGE-variance. The cumulative sum of ranked and normalized TO indices then gives the cumulative fraction of total modeled KGE-variance accounted for by parameters of equal or greater influence (as quantified by TO index). This cumulative sum is shown in column "Cumulative variance accounted for" of Table S5. The results in this column show that 12 SWAT parameters, shaded in gray in Table S5, accounted for over 99% of the total modeled KGE-variance. These 12 parameters were selected as the set of parameters to estimate via calibration, described in the next section.

S4. Watershed model calibration and validation

We calibrated the SWAT watershed model using the SUFI-2 (Sequential Uncertainty FItting Ver. 2) method with SWAT-CUP software (Arnold et al., 2012 b). We also used the add-on parallel processing license purchased from Neprash Technology in 2016 (Rouholahnejad et al., 2012). As put by Santhi et al. (2001), calibration in SWAT should involve some small adjustments to parameters that we have more physical knowledge of, and more substantial adjustments to other parameters of a more empirical and less physical nature. One of the aims of the SUFI-2 method is to obtain calibrated ranges of a user specified set of parameters (i.e., "calibrate" the model) that give ranges in model predictions bracketing as many observations as possible. The observations in this study are monthly stream discharge. The width of the range in model predictions gives the uncertainty in the model, as quantified by the "r-factor" (Yang et al., 2008). The fraction of observations bracketed by the range in model predictions is referred to as the "p-factor" (Abbaspour et al., 2004, 2007). The p-factor can be interpreted as the fraction of observations explained by the model given all sources of uncertainty. For a more technical description of the SUFI-2 method, the reader is referred to Abbaspour et al. (2004, 2007) and Yang et al. (2008).

To implement SUFI-2, the user first supplies a list of parameters, their initial ranges, and the mathematical form (definition) of the objective function. The user then manually applies several iterations of simulations until achieving an r-factor of less than approximately 1. Each iteration consists of a set of N simulations (N = 1000 in this study) that randomly sample parameters over a latin hypercube. A final calibrated model with a p-factor of ≥ 0.8 and r-factor ≤ 1.0 can be considered satisfactory (Abbaspour et al., 2004, 2007). In addition, the single simulation providing the highest objective function value ("best simulation") should conform to the performance criteria given in Moriasi et al. (2007) and Abbaspour et al. (2004, 2007).

For the objective function of calibration, we selected the Kling-Gupta efficiency (KGE) (Gupta et al., 2009) of monthly modeled streamflow, using for observations full natural flows at the watershed outlet (CDEC, 2020 b). We first tried using the Nash-Sutcliffe efficiency (NSE) (Nash and Sutcliffe, 1970) as the objective function but obtained unacceptably high values of percent streamflow bias (PBIAS) ($\geq 15\%$) (Moriasi et al., 2007), even though NSE-values were good (≥ 0.9). We then switched objective functions to KGE and obtained acceptable values of both NSE and PBIAS according to the performance criteria in Moriasi et al. (2007).

In calibrating the SWAT model, we sought to estimate values of parameters having the most influence on the objective function, KGE. To identify the set of the most influential parameters, we conducted the global sensitivity analysis described in section S3. Based on results of that analysis, we selected for calibration the 12 parameters accounting for approximately 99% of total variance in modeled KGE. These parameters are listed in the gray-shaded rows of Table S5.

Two sets of parameter ranges are needed for SUFI-2, *intial ranges* and *absolute ranges*. Initial ranges are the ranges input to SUFI-2 for the first iteration of simulations. Subsequent iterations of SUFI-2 produce shifts in parameter ranges depending on two things: parameter values of the simulation producing the highest objective, termed the "best" simulation, and the diagonal elements of the parameter covariance matrix (Abbaspour et al., 2004). Because of this shift in parameter range between successive SUFI-2 iterations, absolute minimum and maximum limits of parameter ranges, termed "absolute ranges," were defined for each parameter based on either physical plausibility or the literature for parameters of a more empirical nature. We set these absolute ranges equal to the ranges sampled in the sensitivity analysis (Table S4), with the following exception. The upper limit of the absolute range for REVAPMN, which controls the "revap" component of evapotranspiration, was lowered from 3000 to 2000 mm. This change was made to increase availability of water in the shallow aquifer for uptake by deep-rooted plants (Neitsch et al., 2011), providing needed increases in modeled ET during calibration. The absolute ranges are listed in the "Absolute range" columns of Table S6. After some trial and error, we determined the other set of parameter ranges, initial ranges, as follows. We centered the initial ranges on the parameter values producing the highest KGE-value of the sensitivity analysis (section S3). These parameters are listed in the "Best parameter (highest KGE)" column of Table S5 and the "Initial range, center" column of Table S6. We also needed the widths of the intial ranges, defined as maximum − minimum values, to completely define the initial ranges. We set these widths equal to two-thirds of the width of the absolute ranges of parameters. Based on previous experience, we have found that the factor of two-thirds works well by allowing the bounds of the parameter ranges some room to shift during successive SUFI-2 iterations. The initial ranges are listed in the "Initial range" columns of Table S6. We'd like to add a final note on the centering of initial ranges. During preliminary calibration work, we centered the initial ranges on the centers of absolute ranges and set widths of initial ranges to two-thirds of the widths of absolute ranges. This method resulted in SUFI-2 "missing" the best simulations occurring near the limits of the absolute ranges. This became apparent after examining the highest objective function values of the global sensitivity analysis (section S3). We then decided to center the initial ranges on the parameter values producing the highest KGE-value of the sensitivity analysis, as earlier in this paragraph.

The simulation period for model calibration was calendar years 2003–2010, and the simulation period for model validation (i.e., model testing) was calendar years 2011–2019. For both calibration and validation, we applied a 13-calendar year spin-up (warm-up) forced by 10 years of dynamic steady-state weather forcings (for aquifer equilibration) followed by 3 years of real weather data (for soil and plant equilibration). These spin-up periods were 1990–2002 for calibration, 1998–2010 for validation, with the first 10 calendar years of each period assigned to dynamic steady-state weather. The dynamic steady-state weather forcings were the same as those used for the plant spin-up model described in section S2. For a description of the weather products used, and the initial set up of the SWAT model, see section S1 and Table S1.

A total of two SUFI-2 iterations were found sufficient to bring the r-factor down to approximately one. The parameter ranges input to SUFI-2 for this second iteration constitute the "final model", and the specific set of parameters producing the highest objective of calibration

(KGE) constitute the "best model of calibration." Parameter ranges of the final model are listed in the "Final range" columns of Table S6, and parameters of the best model of calibration are listed in the "Best simulation value" (far-right) column of Table S6.

The final model applied to the calibration period had a p-value of 0.94 (i.e., fraction of observations within range of model uncertainty) and an r-factor of 0.85. The best model of calibration applied to the calibration period produced metrics KGE, NSE, and PBIAS of 0.93, 0.93, and +6.2% (model overestimate), respectively. Monthly time series of results from this model are plotted in Figure 2a of the main paper. The final model applied to the validation period had a p-value of 0.90 and an r-factor of 0.71. The best model of calibration applied to the validation period produced metrics KGE, NSE, and PBIAS of 0.89, 0.92, and −2.7% (model underestimate), respectively. Monthly time series of results from this model are plotted in Figure 2b of the main paper. These calibration and validation results are considered overall to be very good based on performance criteria in Moriasi et al. (2007) and Abbaspour et al. (2007).

Table S1. Spatial datasets used in construction of watershed model in ArcSWAT 2012

Dataset	Source	References
Elevation	Digital elevation model (DEM) from the National Elevation Dataset (NED), 1 arc-second resolution	USGS (2013)
Soil	State Soil Geographic (STATSGO) data base accompanying ArcSWAT 2012, scale approximately 1:250,000,	USDA (1994)
Land use	National Land Cover Database (NLCD) 2011, 30-m resolution	USGS (2019)
Precipitation, minimum and maximum air temperature, relative humidity	PRISM AN81d product at daily 2.5-arcminute resolution	Daly et al. (2008, 2015); PRISM Climate Data
Downward solar radiation, wind speed	GridMET product at daily 2.5-arcminute resolution	Abatzoglou (2013); Climatology Lab

Table S2. Parameter values of "base model" manually entered into tables of ArcSWAT project

Parameter name	Description	Table	Value	References
PLAPS	Precipitation lapse rate (mm/km)	sub	114.6	Goulden et al. (2012)
TLAPS	Air temperature lapse rate (°C/km)	sub	−5.3	Goulden et al. (2012)
CANMX	Maximum canopy storage (mm H_20)	hru	1.0	Harpold et al. (2014), Grip and Hällgren (2005), Corbett and Crouse (1968), Wang et al. (2005)
ESCO	Soil evaporation compensation factor	hru	0.51	Best simulation in supplement Table S6 of Jepsen et al. (2018)
SHALLST	Initial depth of water in shallow aquifer (mm)	gw	2000	Set to same value as GWQMN while allowing storage for revap when shallow aquifer storage < GWQMN
GW_DELAY	Groundwater delay time (days)	gw	152	Best simulation in supplement Table S6 of Jepsen et al. (2018)
ALPHA_BF	Baseflow alpha factor (recession constant) (1/days)	gw	0.053	Digital filter program of Arnold et al. (1995) and Arnold and Allen (1999) applied to 1987-2003 daily, full natural streamflow at Pine Flat dam (CDEC, 2020 a)
GWQMN	Threshold depth of water in shallow aquifer required for return flow to occur (mm)	gw	2000	Set to same value as SHALLST while allowing storage for REVAP when shallow aquifer storage < GWQMN
GW_REVAP	Groundwater “revap” coefficient allowing upward movement of water from shallow aquifer to soil and root zone	gw	0.06	Best simulation in supplement Table S6 of Jepsen et al. (2018)
REVAPMN	Threshold depth of water in shallow aquifer for “revap” or percolation to deep aquifer to occur (mm)	gw	1500	Provides 500 mm storage capacity for revap when shallow aquifer storage < GWQMN
RCHRG_DP	Deep aquifer percolation fraction (-)	gw	0.0	Ensures long-term balance between stream-outflow volume and volume of (precipitation − evapotranspiration)
SFTMP	Snowfall temperature (°C)	bsn	2.09	Best simulation in supplement Table S6 of Jepsen et al. (2018)
SMTMP	Snow melt base temperature (°C)	bsn	0.57	Best simulation in supplement Table S6 of Jepsen et al. (2018)
SMFMX	Melt factor for snow on June 21 (mm H_2O $°C^{-1}$ day^{-1})	bsn	3.52	Best simulation in supplement Table S6 of Jepsen et al. (2018)
SMFMN	Melt factor for snow on December 21 (mm H_2O $°C^{-1}$ day^{-1})	bsn	1.60	Best simulation in supplement Table S6 of Jepsen et al. (2018)
TIMP	Snow pack temperature lag factor (-)	bsn	0.60	Best simulation in supplement Table S6 of Jepsen et al. (2018)
SNOCOVMX	Minimum snow water content that corresponds to 100% snow cover	bsn	2393	Regression best fit to data from Guan et al. (2013), shown in Figure S4 of this supplement
SNO50COV	Fraction of snow volume represented by SNOCOVMX that corresponds to 50% snow cover	bsn	0.08781	Regression best fit to data from Guan et al. (2013), shown in Figure S4 of this supplement
RCN	Concentration of nitrogen in rainfall (mg/l)	bsn	1.0	National Trends Network maps by National Atmospheric Deposition Program (NRSP-3)

Table S3. Modifications to plant database of SWAT model (file plant.dat) to more closely simulate biophysical parameters of mature Sierra Nevada forest. Land use categories are from the National Land Cover Database (NLCD) 2011 (USGS, 2019). Definitions: VPD = vapor pressure deficit

Land use (land cover)	Parameter	Definition	Original value	Modified value	References
Evergreen Forest	ALAI_MIN	Minimum leaf area index during dormancy (-)	0.75	1.5	Heiskanen et al. (2012); Liu et al. (2012); Wang and Chen (2012); Tang et al. (2014)
Evergreen Forest	BLAI	Maximum (potential) leaf area index (-)	5.0	5.0	No modification made
Evergreen Forest	FRGMAX	Fraction of maximum stomatal conductance corresponding to 2nd point on stomatal conductance curve	0.75	0.75	No modification made
Evergreen Forest	GSI	Maximum stomatal conductance (m/s) at high solar radiation, low VPD	0.0020	0.0026	Intermediate between SWAT default of 0.002 and value of 0.0032 in Table 1 of Mu et al. (2011)
Evergreen Forest	T_BASE	Minimum (base) temperature for tree growth (°C)	0.0	0.0	No modification made
Evergreen Forest	T_OPT	Optimal temperature for tree growth (°C)	30	10	Mu et al. (2011); Goulden and Bales (2014); Kelly and Goulden (2016)
Shrub/Scrub	ALAI_MIN	Minimum leaf area index during dormancy (-)	0.0	0.5	Shrubs include Ceanothus, manzanita, and buckeye (Giger and Schmitt, 1993), many of which are evergreen
Shrub/Scrub	BLAI	Maximum (potential) leaf area index (-)	2.0	1.5	Tang et al. (2014)
Shrub/Scrub	FRGMAX	Fraction of maximum stomatal conductance corresponding to 2nd point on stomatal conductance curve	0.75	0.75	No modification made
Shrub/Scrub	GSI	Maximum stomatal conductance (m/s) at high solar radiation, low VPD	0.0050	0.0057	Intermediate between SWAT default of 0.005 and value of 0.0065 in Table 1 of Mu et al. (2011)
Shrub/Scrub	T_BASE	Minimum (base) temperature for plant growth (°C)	12	5.0	See note (1), below
Shrub/Scrub	T_OPT	Optimal temperature for tree growth (°C)	25	20	See note (2), below
Barren Land	BLAI	Maximum (potential) leaf area index (-)	1.5	0.1	"Barren land" in NLCD database presumably has almost no vegetation cover

Table S3 notes: (1): 5°C is intermediate between SWAT default of 12 and value of −1.0 found from adding 6.6°C, the average difference between average and minimum daily air temperature (not shown), to the value of Tmin_close for shrubs in Mu et al. (2011). (2): 20°C is intermediate between SWAT default of 25 and value of 15 found from adding 6.6°C, the average difference between average and minimum daily air temperature (not shown), to the value of Tmin_open for shrubs in Mu et al. (2011).

Table S4. SWAT model parameters varied in global sensitivity analysis using Sobol method (Saltelli et al., 2000) in SALib (Herman and Usher, 2017). The objective function analyzed was Kling-Gupta efficiency (Gupta et al., 2009) of monthly SWAT modeled streamflow. Parameters were scaled globally by the following scaling types: v = parameter replacement, r = parameter multiplication by (1 + value), a = addition to parameter.

Parameter name	Definition	Scaling type	Minimum of range	Maximum of range	References
CH_N(2)	Manning's "n" value for the main channel	v	0.01	0.2	Arnold et al. (2012 a)
CH_K(2)	Effective hydraulic conductivity in main channel alluvium (mm/hr)	v	0.0	150	Zhang et al. (2011); Arnold et al. (2012 a); Ficklin et al. (2013)
GW_DELAY	Groundwater delay time (days)	v	0.01	220	Jeong et al. (2010); Zhang et al. (2011); Ficklin et al. (2013)
GW_REVAP	Groundwater “revap” coefficient allowing upward movement of water from shallow aquifer to soil and root zone	v	0.02	0.2	Arnold et al. (2012 a)
REVAPMN	Threshold depth of water in shallow aquifer for “revap” or percolation to deep aquifer to occur (mm)	v	1000	3000	Taken to be centered about parameters GWQMN and SHALLST
CANMX	Maximum canopy storage (mm H_20)	v	0.0	4.0	Grip and Hällgren (2005), Corbett and Crouse (1968), Wang et al. (2005)
FRGMAX	Fraction of maximum stomatal conductance corresponding to 2nd point on stomatal conductance curve	r	−0.25	0.25	Mu et al. (2011)
GSI	Maximum stomatal conductance (m/s) at high solar radiation, low VPD	r	−0.25	0.25	Range covers SWAT default of 0.002 and value of 0.0032 in Table 1 of Mu et al. (2011)
BLAI	Maximum (potential) leaf area index (-)	r	−0.25	0.25	Tang et al. (2014)
ALAI_MIN	Minimum leaf area index during dormancy (-)	r	−0.25	0.25	Tang et al. (2014)
T_BASE	Minimum (base) temperature for plant growth (°C)	a	−5.0	5.0	Creates range that does not overlap with range of paramter T_OPT
T_OPT	Optimal temperature for tree growth (°C)	a	−5.0	5.0	Goulden and Bales (2014); Kelly and Goulden (2016)
SFTMP	Snowfall temperature (°C)	v	−5.0	5.0	Daly et al. (2000); Dai (2008); Arnold et al. (2012 a)
SMFMN	Melt factor for snow on December 21 (mm H_2O °C^{-1} day^{-1})	v	0.0	8.0	Daly et al. (2000); Fontaine et al. (2002); Abbaspour et al. (2007); Arnold et al. (2012 a); Ficklin et al. (2013); Jepsen et al. (2016)
SMFMX	Melt factor for snow on June 21 (mm H_2O °C^{-1} day^{-1})	v	0.0	8.0	Daly et al. (2000); Fontaine et al. (2002); Abbaspour et al. (2007); Arnold et al. (2012 a); Ficklin et al. (2013); Jepsen et al. (2016)

Table S4 – continued.

Parameter name	Definition	Scaling type	Minimum	Maximum	References
SMTMP	Snow melt base temperature (°C)	v	−5.0	5.0	Daly et al. (2000); Fontaine et al. (2002); Abbaspour et al. (2007); Arnold et al. (2012 a); Ficklin et al. (2013)
TIMP	Snow pack temperature lag factor (-)	v	0.01	1.0	Arnold et al. (2012 a)
EPCO	Plant uptake compensation factor	v	0.01	1.0	Arnold et al. (2012 a)
ESCO	Soil evaporation compensation factor	v	0.01	1.0	Arnold et al. (2012 a)
SOL_AWC()	Available water capacity of a soil layer (mm H_2O/mm soil)	r	−0.25	0.25	USDA (1999); Jeong et al. (2010); Zhang et al. (2011); Qiu et al. (2012); Ficklin et al. (2013)
SOL_BD()	Moist bulk density of a soil layer (g cm^{-3})	r	−0.1	0.1	Arnold et al. (2012 a)
SOL_K()	Saturated hydraulic conductivity of a soil layer (mm/hr)	r	−0.5	0.5	Freeze and Cherry (1979); USDA (1999)
SOL_Z()	Depth from soil surface to bottom of a soil layer (mm)	r	−0.5	0.5	Watson and Putz (2014); see note (1), below
CN2	Initial SCS runoff curve number for soil moisture condition II	r	−0.25	0.25	Van Liew et al. (2005); Zhang et al. (2011); Qiu et al. (2012); Ficklin et al. (2013); Watson and Putz (2014)
OV_N	Manning's "n" value for overland flow	r	−0.25	0.25	Arnold et al. (2012 a)
SURLAG	Surface runoff lag coefficient	v	0.01	15	Jeong et al. (2010); Zhang et al. (2011); Arnold et al. (2012 a)

Table S4 notes: (1) multiplicative factor of 1.38 needed to get ET high enough during preliminary, manual calibration leading to Jepsen et al. (2018).

Table S5. Results of Sobol sensitivity analysis showing contribution of each SWAT parameter to total modeled variance in Kling-Gupta efficiency (KGE) (Gupta et al., 2009) of monthly streamflow. For parameter definitions, see Table S4. Analysis carried out using the SALib package for Python (Herman and Usher, 2017). "Total order index" (TO index) is the sum of all sensitivity indices involving the parameter, also known as "total sensitivity index" (Saltelli et al, 2000). "Cumulative variance accounted for" is the fraction of total modeled KGE-variance explained by parameters of equal or greater TO index, calculated by forming a running total of TO indices normalized to unity. The 12 parameters gray-shaded below accounted for over 99% of total modeled KGE-variance. "Best parameter" is the value of the parameter scaling factor from the simulation with the highest KGE-value of 0.894 (for scaling types, see Table S4).

Parameter name	Total order index	Confidence interval, total order index	Best parameter (highest KGE)	Cumulative variance accounted for
SMFMX	0.6139	0.0844	4.902	0.4343
SFTMP	0.2495	0.0588	4.780	0.6108
CH_K(2)	0.2225	0.0493	37.13	0.7681
SMTMP	0.1367	0.0413	−0.0635	0.8648
REVAPMN	0.0484	0.0211	1403	0.8990
SMFMN	0.0454	0.0431	4.676	0.9311
CH_N(2)	0.0408	0.0177	0.0348	0.9600
GW_DELAY	0.0126	0.0069	185.3	0.9690
SOL_Z()	0.0104	0.0076	0.4780	0.9763
TIMP	0.0085	0.0127	0.6205	0.9824
SOL_K()	0.0083	0.0054	−0.4438	0.9882
GW_REVAP	0.0069	0.0091	0.1660	0.9931
CN2	0.0059	0.0077	0.0505	0.9973
CANMX	0.0013	0.0041	1.049	0.9982
GSI	0.0008	0.0015	−0.1965	0.9987
T_BASE	0.0007	0.0012	-1.821	0.9992
SOL_AWC()	0.0004	0.0028	0.2375	0.9995
ESCO	0.0003	0.0009	0.5780	0.9997
EPCO	0.0002	0.0016	0.5035	0.9999
SOL_BD()	0.0001	0.0033	-0.0567	1.0000
BLAI	0.0000	0.0009	-0.0559	1.0000
FRGMAX	0.0000	0.0001	-0.0022	1.0000
ALAI_MIN	0.0000	0.0008	-0.2170	1.0000
SURLAG	0.0000	0.0000	4.028	1.0000
OV_N	0.0000	0.0000	-0.0090	1.0000
T_OPT	-0.0001	0.0008	3.784	1.0000

Table S6. Parameter ranges of calibrated SWAT model found using SWAT-CUP with the SUFI-2 (Sequential Uncertainty FItting Ver. 2) method (Abbaspour et al., 2007; Yang et al., 2008; Arnold et al., 2012 b). For parameter definitions, see Table S4. Values listed in this table are expressed as the scaling factors defined in Table S4. Values in column "Initial range, center" were taken from "Best parameter (highest KGE)" column of Table S5.

Parameter name	**Absolute range**, minimum	**Absolute range**, maximum	**Initial range**, center	**Initial range**, minimum	**Initial range**, maximum	**Final range**, minimum	**Final range**, maximum	Best simulation value
SMFMX	0.0	8.0	4.902	2.236	7.569	1.677	5.605	2.260
SFTMP	−5.0	5.0	4.780	−1.665	5.0	1.232	5.0	3.453
CH_K(2)	0.0	150	37.13	0.0	99.98	1.971	67.33	2.265
SMTMP	−5.0	5.0	−0.0635	−3.397	3.270	−2.525	1.338	−1.067
REVAPMN	1000	2000	1403	1070	1737	1000	1441	1408
SMFMN	0.0	8.0	4.676	2.009	7.342	0.0	4.773	1.167
CH_N(2)	0.01	0.2	0.0348	0.01	0.1366	0.0524	0.1373	0.0951
GW_DELAY	0.01	220	185.3	73.33	220	67.20	169.1	98.93
SOL_Z()	−0.5	0.5	0.4780	−0.1665	0.5	−0.0124	0.3292	0.3072
TIMP	0.01	1.0	0.6205	0.2905	0.9505	0.4676	0.8217	0.4932
SOL_K()	−0.5	0.5	−0.4438	−0.5	0.1667	−0.4549	−0.0405	−0.4074
GW_REVAP	0.02	0.2	0.1660	0.0800	0.2	0.1320	0.2	0.1463

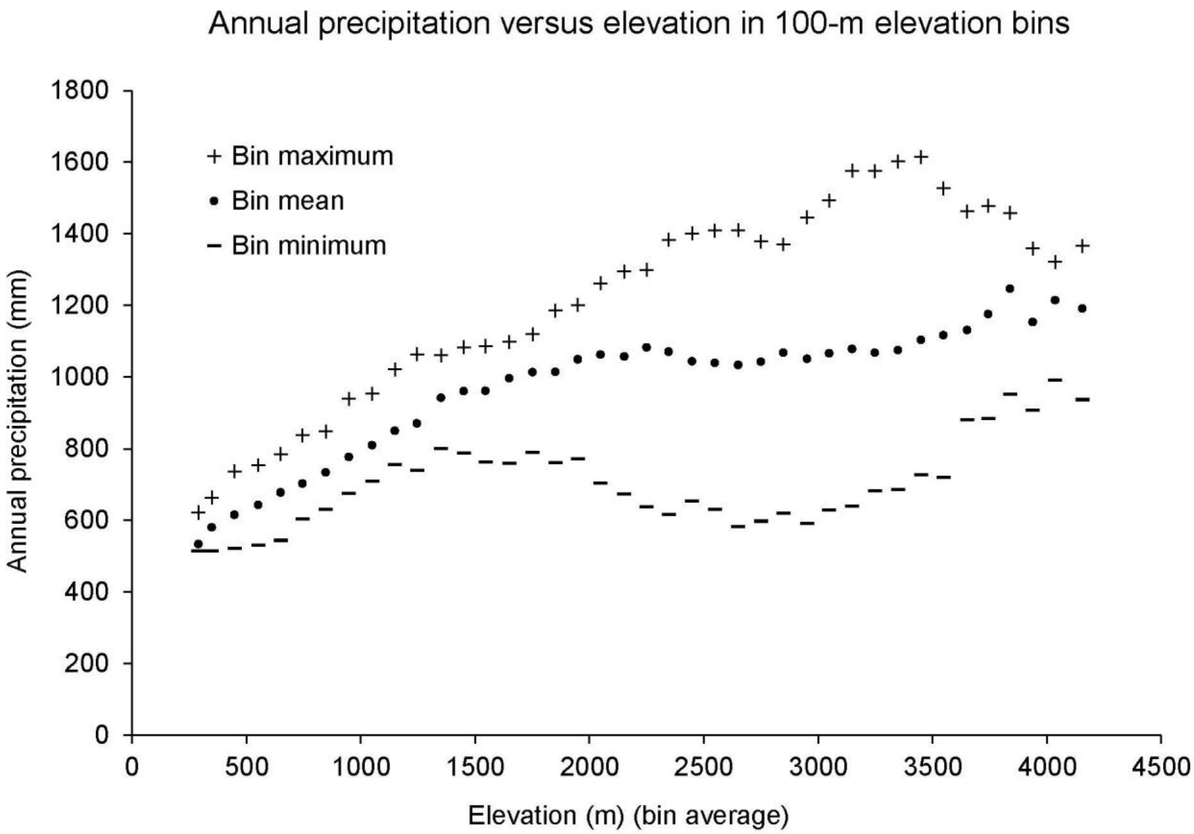

Figure S1. Annual precipitation versus elevation in upper Kings River watershed in 100-m elevation bins. Precipitation based on 1981–2010 climatic normals from the PRISM Norm81d product (Daly et al., 2008; PRISM Climate Data), elevations from USGS (2013).

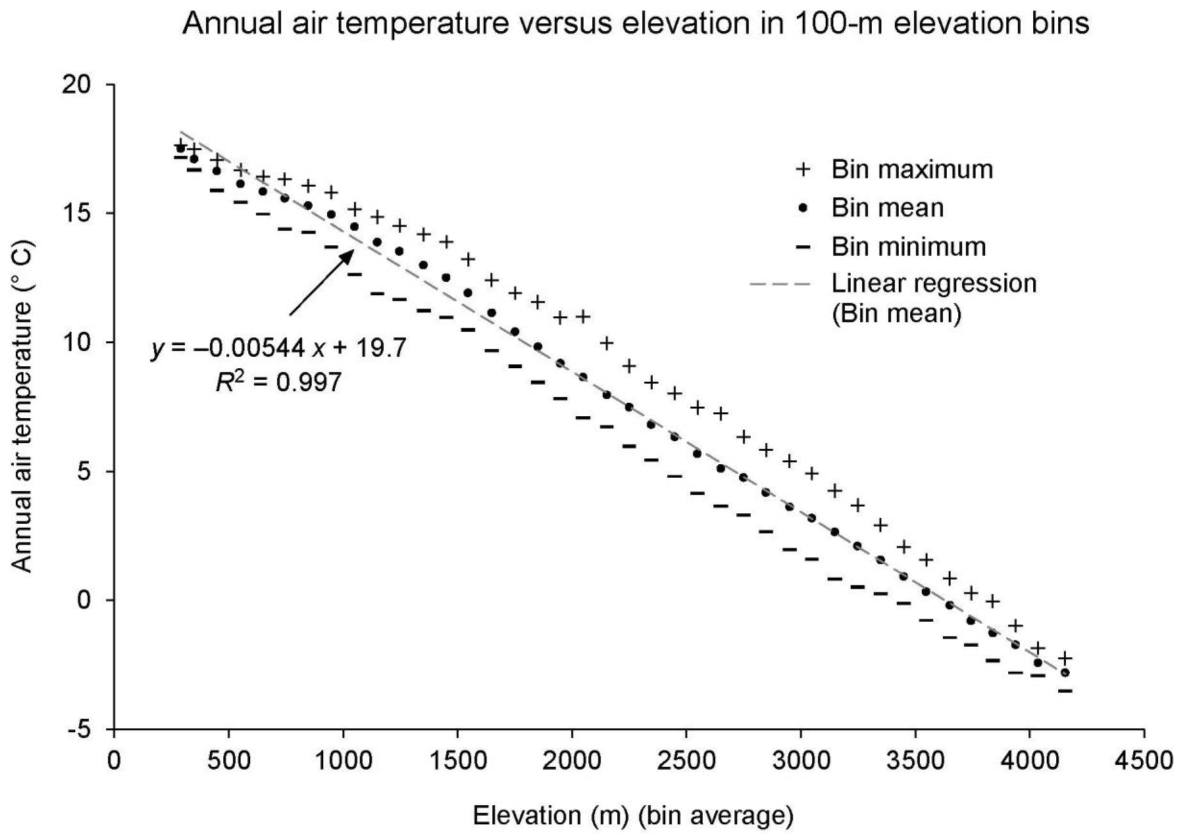

Figure S2. Annual air temperature versus elevation in upper Kings River watershed in 100-m elevation bins. Temperatures based on 1981–2010 climatic normals from the PRISM Norm81d product (Daly et al., 2008; PRISM Climate Data), elevations from USGS (2013).

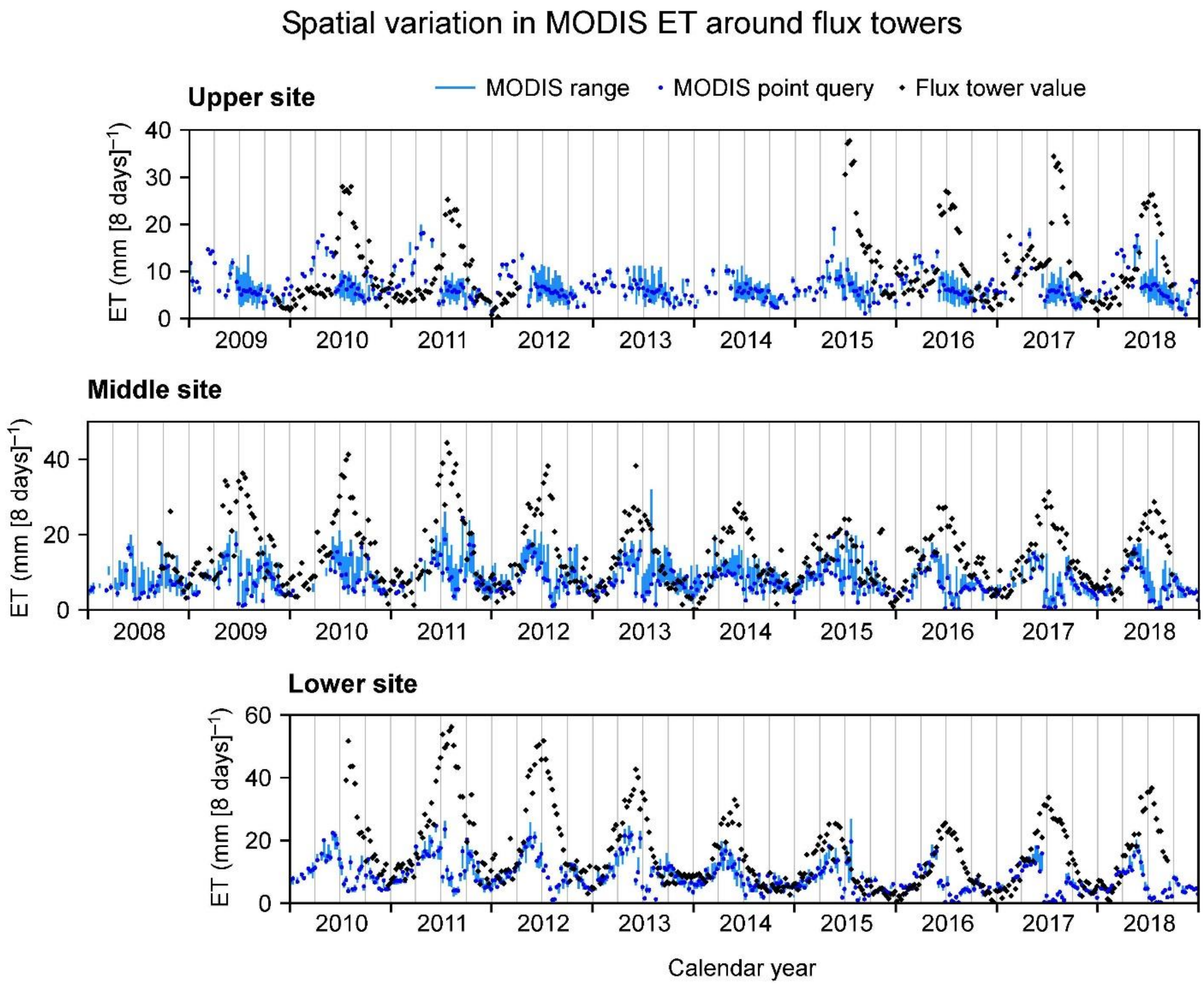

Figure S3. Ranges in MODIS 8-day ET within or touching a 500-m radius buffer around each flux tower location. Ranges in MODIS ET within/touching buffer are given by blue bars and denoted "MODIS range" in legend. Values of MODIS ET used in this study are from MODIS cells containing flux tower locations, plotted above as blue circles and denoted "MODIS point query" in legend. Flux tower ET-values shown as black diamonds. We defined MODIS ET-error as the difference between the MODIS point query and the flux tower value. These errors are much less than differences between MODIS point queries and limits of MODIS ranges, showing that the values we used for MODIS ET-error would not be sensitive to spatial variation in MODIS ET within a plausible flux tower footprint.

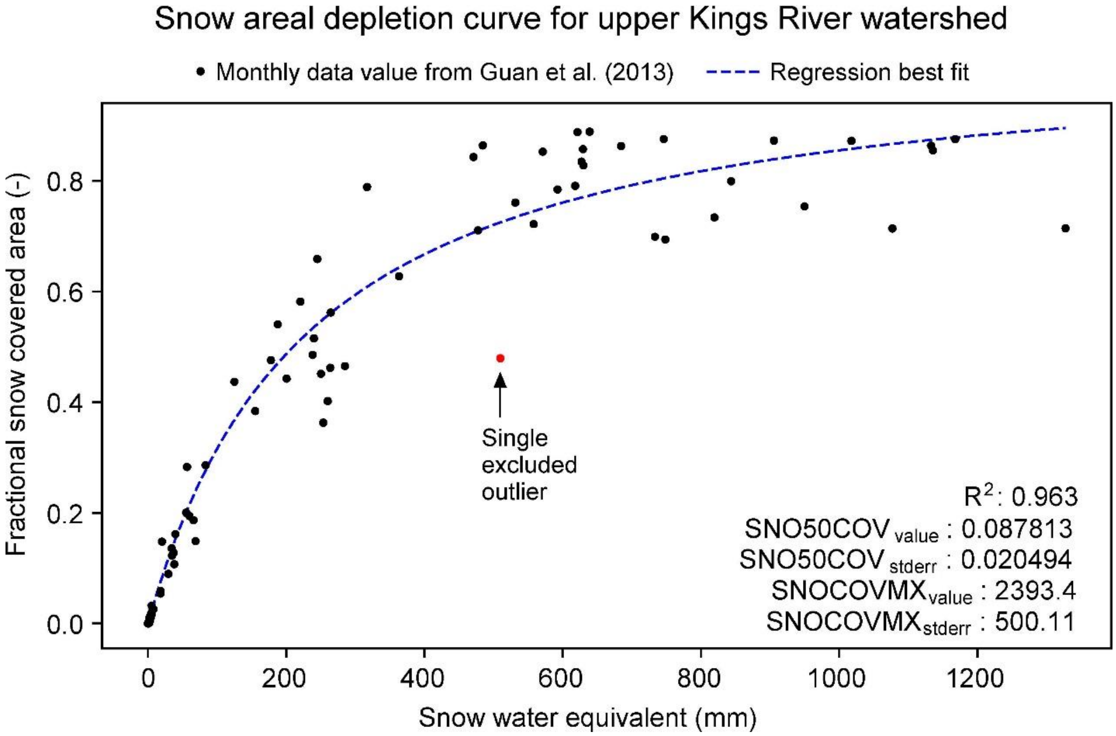

Figure S4. SWAT model parameterization of snow areal depletion curve for upper Kings River watershed. Values of fractional snow covered area and snow water equivalent are monthly averages from Guan et al. (2013) at watershed elevations above 2500 m. Data values are fit to the snow areal depletion equation 1:2.4.2 in Neitsch et al. (2011). Fitting was performed using the curve_fit function of the scipy.optimize module for Python. One outlier was excluded (red circle) having a residual greater than three standard deviations from the best-fit solution.

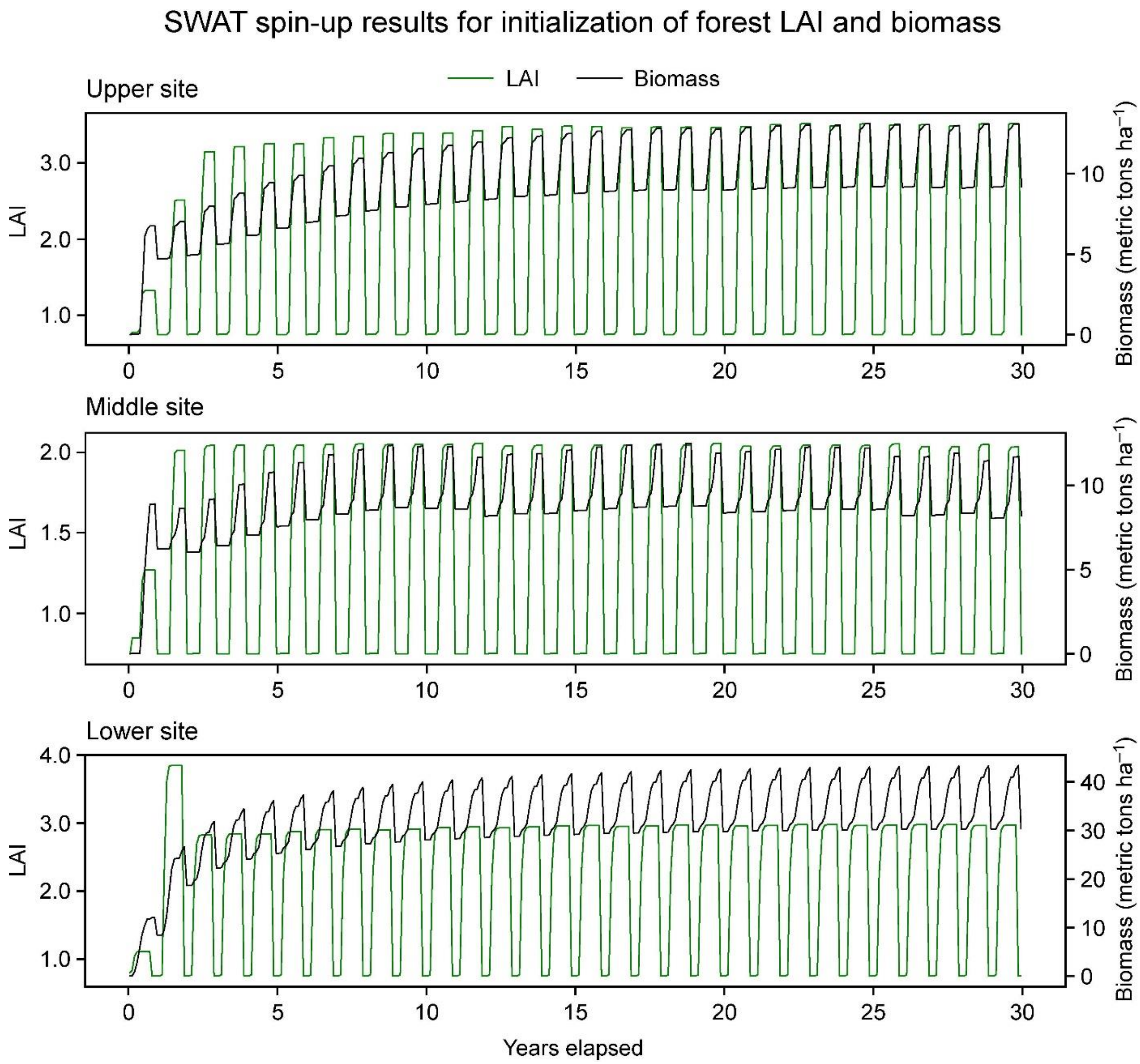

Figure S5. Monthly leaf area index (LAI) and biomass from 30-year spin-up simulation of SWAT base model to steady-state weather conditions. Final LAI and biomass from these spin-up simulations were used to initialize the "plant spin-up model" (section S2). Dynamic steady-state weather were used for these spin-up simulations consisting of daily averages of products listed in Table S1 during the 2000–2019 period.

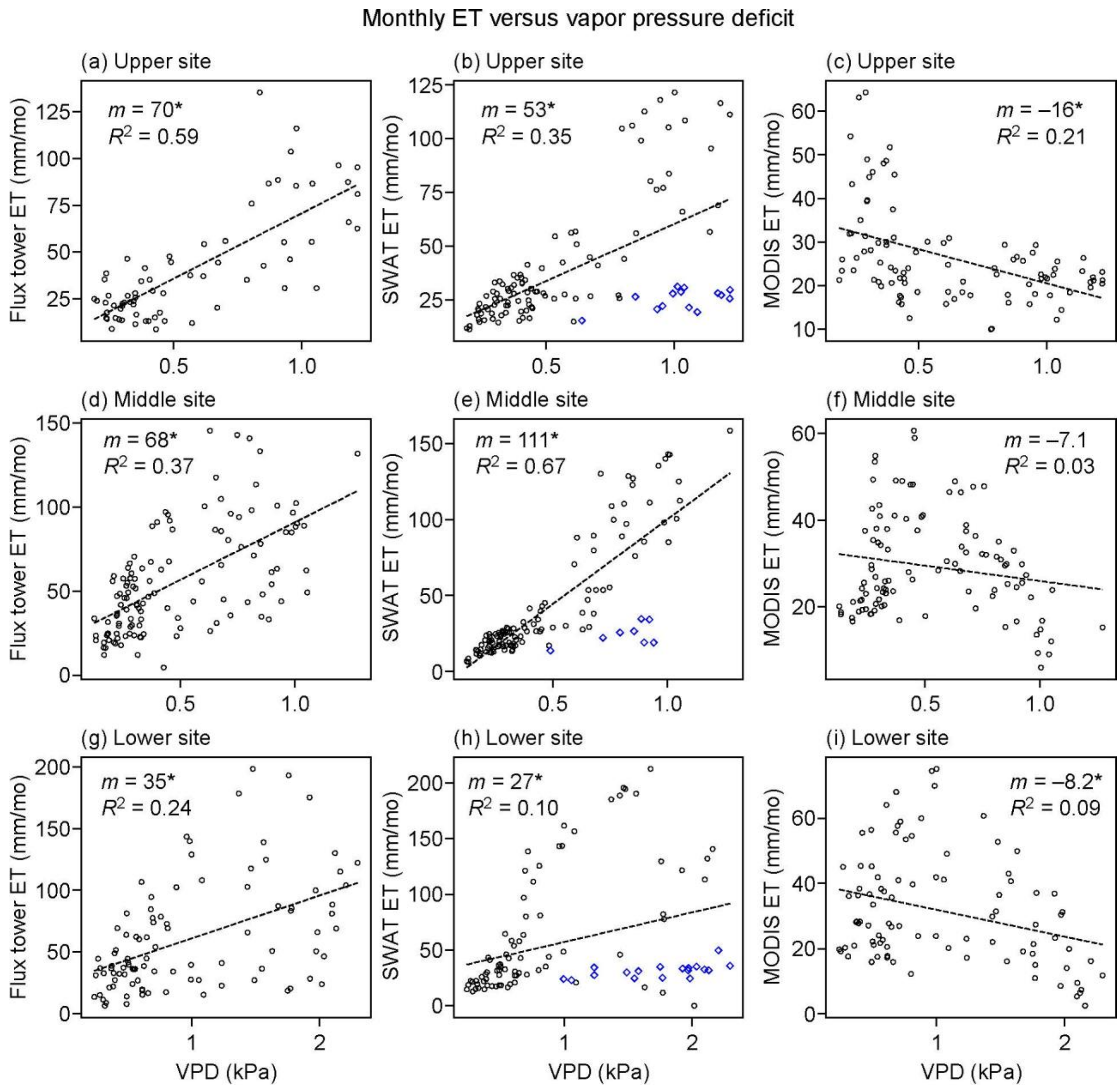

Figure S6. Monthly ET versus vapor pressure deficit (VPD) from different data sources at the (a–c) upper site, (d–f) middle site, and (g–i) lower site. Dashed lines are best fits from linear regression. *m* = slope of regression best-fit with asterisk where *p*-value < 0.05, R^2 = coefficient of determination of best-fit. In center column, SWAT modeled ET supplied primarily by aquifer water ("REVAP") are plotted as blue-colored diamond symbols.

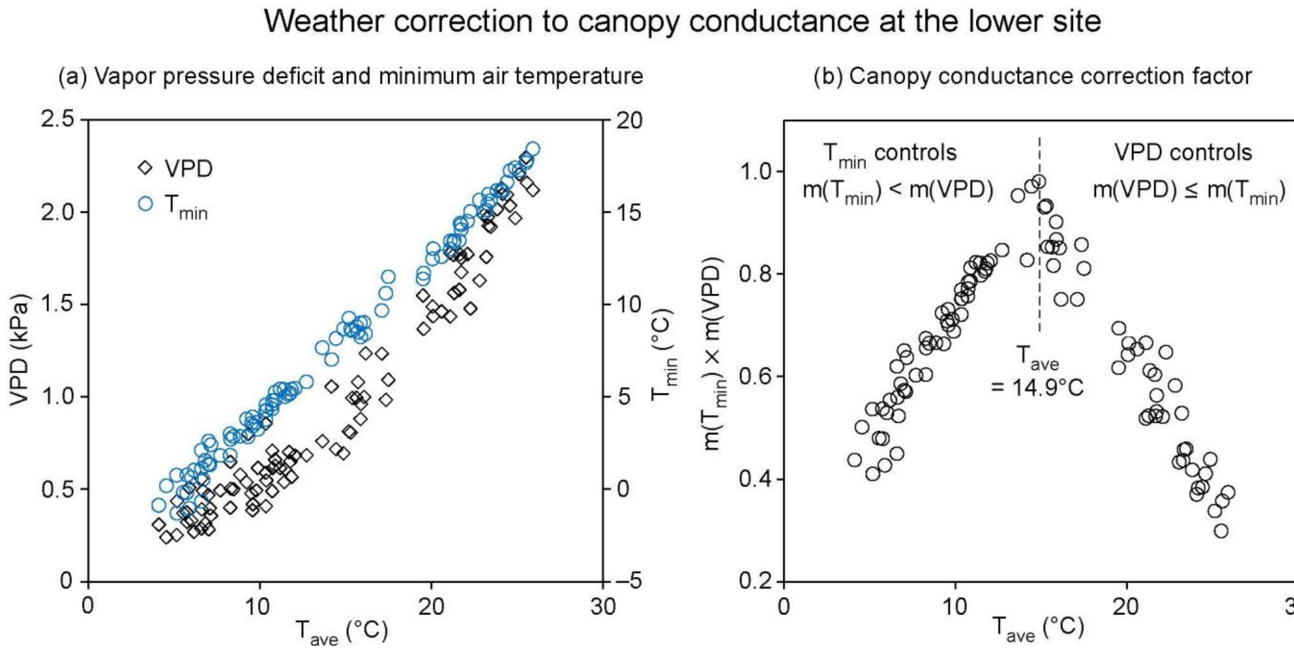

Figure S7. Weather correction to canopy conductance at the lower site based on equation 5 in Mu et al. (2007) and biome properties of evergreen needleleaf forest in Table 1 of Mu et al. (2011). Weather variables used for the conductance correction are vapor pressure deficit (VPD) and minimum air temperature (T_{min}) from PRISM AN81d product (Daly et al. 2008, 2015; PRISM Climate Data) masked to the watershed subbasin containing the SWAT Hydrologic Response Unit at the lower site (Figure 1). (a) Monthly VPD and T_{min} versus average air temperature (T_{ave}). (b) Canopy conductance correction factor (y-axis) versus T_{ave}. In the MODIS ET algorithm, canopy conductance is scaled by the correction factor given by $m(T_{min}) \times m(VPD)$ (equation 5 in Mu et al., 2007). For weather conditions shown, T_{min} controls the conductance correction when $m(T_{min}) < m(VPD)$ and VPD controls the conductance correction when $m(VPD) \leq m(T_{min})$. The transition from T_{min}- to VPD-controlled canopy conductance occurs at T_{ave} = 14.9°C.

References

Abatzoglou, J. T. (2013). Development of gridded surface meteorological data for ecological applications and modelling. International Journal of Climatology, 33(1), 121–131. https://doi.org/10.1002/joc.3413

Abbaspour, K. C., Johnson, C. A., & van Genuchten, M. Th. (2004). Estimating uncertain flow and transport parameters using a sequential uncertainty fitting procedure. Vadose Zone Journal, 3(4), 1340. https://doi.org/10.2136/vzj2004.1340

Abbaspour, K. C., Yang, J., Maximov, I., Siber, R., Bogner, K., Mieleitner, J., Zobrist, J., & Srinivasan, R. (2007). Modelling hydrology and water quality in the pre-alpine/alpine Thur watershed using SWAT. Journal of Hydrology, 333(2–4), 413–430. https://doi.org/10.1016/j.jhydrol.2006.09.014

Arnold, J. G., Allen, P. M., Muttiah, R., & Bernhardt, G. (1995). Automated base flow separation and recession analysis techniques. Ground Water, 33(6), 1010–1018. https://doi.org/10.1111/j.1745-6584.1995.tb00046.x

Arnold, J. G., & Allen, P. M. (1999). Automated methods for estimating baseflow and ground water recharge from streamflow records. Journal of the American Water Resources Association, 35(2), 411–424. https://doi.org/10.1111/j.1752-1688.1999.tb03599.x

Arnold, J. G., Kiniry, J. R., Srinivasan, R., Williams, J. R., Haney, E.B., & Neitsch, S. L. (2012 a). Soil & Water Assessment Tool Input/Output Documentation Version 2012. Report TR-439, Texas Water Resources Institute, 654 p. Retrieved on 13 Mar 2015 from https://swat.tamu.edu/

Arnold, J. G., Moriasi, D. N., Gassman, P. W., Abbaspour, K. C., White, M. J., Srinivasan, R., Santhi, C., Harmel, R. D., van Griensven, A., Van Liew, M. W., Kannan, N., & Jha, M. K. (2012 b). SWAT: Model use, calibration, and validation. Transactions of the ASABE, 55(4), 1491–1508. https://doi.org/10.13031/2013.42256

CDEC (2020 a). Daily full natural streamflow of Kings River at Pine Flat Dam, station ID PNF. Station operated by U.S. Army Corps of Engineers, data provided by California Data Exchange Center, California Department of Water Resources. Retrieved on 21 Apr 2020 from http://cdec.water.ca.gov/dynamicapp/wsSensorData

CDEC (2020 b). Monthly full natural streamflow of Kings River at Pine Flat Dam, station ID KGF. Station operated by U.S. Army Corps of Engineers, data provided by California Data Exchange Center, California Department of Water Resources. Retrieved on 15 Oct 2020 from http://cdec.water.ca.gov/dynamicapp/wsSensorData

Climatology Lab. Daily High-Spatial Resolution (~4-km, 1/24th Degree) Surface Meteorological Data covering the Contiguous U.S. from 1979-Yesterday. University of California, Merced. Available online: http://www.climatologylab.org/gridmet.html (accessed on 10 February 2020).

Corbett, E. S., & Crouse, R. P. (1968). Rainfall interception by annual grass and chaparral...losses compared (U.S. Forest Service Research Paper PSW-48; 12 pp.). Pacific Southwest Forest and Range Experiment Station; Retrieved from https://www.fs.fed.us/psw/publications/documents/psw_rp048/psw_rp048.pdf on 22 April 2020.

Dai, A. (2008). Temperature and pressure dependence of the rain-snow phase transition over land and ocean. Geophysical Research Letters, 35(12), L12802. https://doi.org/10.1029/2008GL033295

Daly, C., Halbleib, M., Smith, J. I., Gibson, W. P., Doggett, M. K., Taylor, G. H., Curtis, J., & Pasteris, P. P. (2008). Physiographically sensitive mapping of climatological temperature and precipitation across the conterminous United States. International Journal of Climatology, 28(15), 2031–2064. https://doi.org/10.1002/joc.1688

Daly, C., Smith, J. I., & Olson, K. V. (2015). Mapping atmospheric moisture climatologies across the conterminous United States. PLoS ONE, 10(10), e0141140. https://doi.org/10.1371/journal.pone.0141140

Daly, S. F., Davis, R., Ochs, E., & Pangburn, T. (2000). An approach to spatially distributed snow modelling of the Sacramento and San Joaquin basins, California. Hydrological Processes, 14(18), 3257–3271. https://doi.org/10.1002/1099-1085(20001230)14:18<3257::AID-HYP199>3.0.CO;2-Z

Ficklin, D. L., Stewart, I. T., & Maurer, E. P. (2013). Effects of climate change on stream temperature, dissolved oxygen, and sediment concentration in the Sierra Nevada in California. Water Resources Research, 49(5), 2765–2782. https://doi.org/10.1002/wrcr.20248

Fontaine, T. A., Cruickshank, T. S., Arnold, J. G., & Hotchkiss, R. H. (2002). Development of a snowfall–snowmelt routine for mountainous terrain for the soil water assessment tool (SWAT). Journal of Hydrology, 262(1–4), 209–223. https://doi.org/10.1016/S0022-1694(02)00029-X

Freeze, R. A, & Cherry, J. A. (1979) Groundwater. Prentice Hall, Englewood Cliffs, NJ, 604 p.

Giger, D.R., and G.J. Schmitt (1993). Soil survey of Sierra National Forest area, California. U.S. Department of Agriculture, Forest Service in cooperation with Soil Conservation Service (presently Natural Resources Conservation Service) and the Regents of the University of California (Agricultural Experiment Station), 150 p. (plus maps). Retrieved on 19 Sep 2018 from https://www.nrcs.usda.gov/Internet/FSE_MANUSCRIPTS/california/sierraNFCA1983/.

Goulden, M. L., Anderson, R. G., Bales, R. C., Kelly, A. E., Meadows, M., & Winston, G. C. (2012). Evapotranspiration along an elevation gradient in California’s Sierra Nevada. Journal of Geophysical Research: Biogeosciences, 117(G3), G03028. https://doi.org/10.1029/2012JG002027

Goulden, M. L., & Bales, R. C. (2014). Mountain runoff vulnerability to increased evapotranspiration with vegetation expansion. Proceedings of the National Academy of Sciences, 111(39), 14071–14075. https://doi.org/10.1073/pnas.1319316111

Grip, H., & Hällgren, J-E. (2005). Water cycling in coniferous forest ecosystems. In: Andersson, F. (Ed.), Ecosystems of the World 6: Coniferous Forests, p. 385-426, Elsevier, Amsterdam, The Netherlands, ISBN 978-0-444-81627-6.

Guan, B., Molotch, N. P., Waliser, D. E., Jepsen, S. M., Painter, T. H., & Dozier, J. (2013). Snow water equivalent in the Sierra Nevada: Blending snow sensor observations with snowmelt model simulations. Water Resources Research, 49(8), 5029–5046. https://doi.org/10.1002/wrcr.20387

Gupta, H. V., Kling, H., Yilmaz, K. K., & Martinez, G. F. (2009). Decomposition of the mean squared error and NSE performance criteria: Implications for improving hydrological modelling. Journal of Hydrology, 377(1–2), 80–91. https://doi.org/10.1016/j.jhydrol.2009.08.003

Harpold, A. A., Guo, Q., Molotch, N., Brooks, P. D., Bales, R., Fernandez-Diaz, J. C., Musselman, K. N., Swetnam, T. L., Kirchner, P., Meadows, M. W., Flanagan, J., & Lucas, R. (2014). LiDAR-derived snowpack data sets from mixed conifer forests across the Western United States. Water Resources Research, 50(3), 2749–2755. https://doi.org/10.1002/2013WR013935

Heiskanen, J., Rautiainen, M., Stenberg, P., Mõttus, M., Vesanto, V.-H., Korhonen, L., & Majasalmi, T. (2012). Seasonal variation in MODIS LAI for a boreal forest area in Finland. Remote Sensing of Environment, 126, 104–115. https://doi.org/10.1016/j.rse.2012.08.001

Herman, J., & Usher, W. (2017). SALib: An open-source Python library for sensitivity analysis. The Journal of Open Source Software, 2(9), 97. https://doi.org/10.21105/joss.00097.

Jeong, J., Kannan, N., Arnold, J., Glick, R., Gosselink, L., & Srinivasan, R. (2010). Development and integration of sub-hourly rainfall–runoff modeling capability within a watershed model. Water Resources Management, 24(15), 4505–4527. https://doi.org/10.1007/s11269-010-9670-4

Jepsen, S. M., Harmon, T. C., Hunsaker, C. T., & Meadows, M.W. (2016). Hydrogeologic influence on changes in snowmelt runoff with climate warming: Numerical experiments on a mid-elevation catchment in the Sierra Nevada, USA. Journal of Hydrology, 533, 332–342, https://doi.org/10.1016/j.jhydrol.2015.12.010

Jepsen, S. M., Harmon, T. C., Ficklin, D. L., Molotch, N. P., & Guan, B. (2018). Evapotranspiration sensitivity to air temperature across a snow-influenced watershed: Space-for-time substitution versus integrated watershed modeling. Journal of Hydrology, 556, 645–659. https://doi.org/10.1016/j.jhydrol.2017.11.042

Kelly, A. E., & Goulden, M. L. (2016). A montane Mediterranean climate supports year-round photosynthesis and high forest biomass. Tree Physiology, 36(4), 459–468. https://doi.org/10.1093/treephys/tpv131

Liu, Z., Jin, G., & Qi, Y. (2012). Estimate of Leaf Area Index in an old-growth mixed broadleaved-Korean pine Forest in northeastern China. PLoS ONE, 7(3), e32155. https://doi.org/10.1371/journal.pone.0032155

Moriasi, D. N., Arnold, J. G., Van Liew, M. W., Bingner, R. L., Harmel, R. D., & Veith, T. L. (2007). Model evaluation guidelines for systematic quantification of accuracy in watershed simulations. Transactions of the ASABE, 50(3), 885–900. https://doi.org/10.13031/2013.23153

Mu, Q., Zhao, M., & Running, S. W. (2011). Improvements to a MODIS global terrestrial evapotranspiration algorithm. Remote Sensing of Environment, 115(8), 1781–1800. Remote_Sensing. https://doi.org/10.1016/j.rse.2011.02.019

Murray, F. W. (1967). On the computation of saturation vapor pressure. Journal of Applied Meteorology, 6(1), 203–204. https://doi.org/10.1175/1520-0450(1967)006<0203:OTCOSV>2.0.CO;2

Nash, J. E., & Sutcliffe, J. V. (1970). River flow forecasting through conceptual models: Part 1. A discussion of principles. Journal of Hydrology, 10(3), 282–290. https://doi.org/10.1016/0022-1694(70)90255-6

National Atmospheric Deposition Program (NRSP-3). 2020. NADP Program Office, Wisconsin State Laboratory of Hygiene, 465 Henry Mall, Madison, WI 53706. Last accessed on 27 Oct 2020 at http://nadp.slh.wisc.edu/

Neitsch, S. L., Arnold, J. G., Kiniry, J. R., & Williams, J. R. (2011). Soil and Water Assessment Tool Theoretical Documentation Version 2009 (Technical Report No. 406; 618 pp.). Texas Water Resources Institute; https://swat.tamu.edu/media/99192/swat2009-theory.pdf

PRISM Climate Data. Northwest Alliance for Computational Science and Engineering, Oregon State University, Corvallis. Available online: http://prism.oregonstate.edu (accessed on 09 October 2020).

Qiu, L., Zheng, F., & Yin, R. (2012). SWAT-based runoff and sediment simulation in a small watershed, the loessial hilly-gullied region of China: Capabilities and challenges. International Journal of Sediment Research, 27(2), 226–234. https://doi.org/10.1016/S1001-6279(12)60030-4

Rouholahnejad, E., Abbaspour, K. C., Vejdani, M., Srinivasan, R., Schulin, R., & Lehmann, A. (2012). A parallelization framework for calibration of hydrological models. Environmental Modelling & Software, 31, 28–36. https://doi.org/10.1016/j.envsoft.2011.12.001

Saltelli, A., Chan, K., & Scott, E. M. (Eds.) (2000). Sensitivity Analysis. John Wiley & Sons Ltd., Chichester, England, 475 p., ISBN 0-471-99892-3.

Santhi, C., Arnold, J. G., Williams, J. R., Dugas, W. A., Srinivasan, R., & Hauck, L. M. (2001). Validation of the SWAT model on a large river basin with point and nonpoint sources. Journal of the American Water Resources Association, 37(5), 1169–1188. https://doi.org/10.1111/j.1752-1688.2001.tb03630.x

Tang, H., Dubayah, R., Brolly, M., Ganguly, S., & Zhang, G. (2014). Large-scale retrieval of leaf area index and vertical foliage profile from the spaceborne waveform lidar (GLAS/ICESat). Remote Sensing of Environment, 154, 8–18. https://doi.org/10.1016/j.rse.2014.08.007

USDA (1994). State Soil Geographic (STATSGO) data base: Data use information. U.S. Department of Agriculture, Natural Resources Conservation Service, Miscellaneous Publication Number 1492, 113 pp. Retrieved on 16 Dec 2016 from http://www.fsl.orst.edu/pnwerc/wrb/metadata/soils/statsgo.pdf

USDA (1999). Rosetta version 1.0 Windows 95/98 program to estimate unsaturated hydraulic properties. United State Department of Agriculture, Agricultural Research Service. Accessed on 06 Aug 2013 at http://www.ars.usda.gov/News/docs.htm?docid=8953.

USGS (2013). National Elevation Dataset (NED) 1 arc-second 2013 1 x 1 degree ArcGrid. U.S. Geological Survey, Reston, VA. Retrieved on 12 Nov 2014 from https://nationalmap.gov/

USGS (2019). NLCD 2011 Land Cover Conterminous United States. U.S. Geological Survey, Sioux Falls, SD. Retrieved on 7 Apr 2020 from https://www.mrlc.gov/.

Van Liew, M. W., Arnold, J. G., & Bosch, D. D. (2005). Problems and potential of autocalibrating a hydrologic model. Transactions of the ASAE, 48(3), 1025–1040. https://doi.org/10.13031/2013.18514

Wang, R., & Chen, J. M. (2012). Seasonal leaf area index variations derived from needle growth and fall measurements in two eastern white pine (Pinus Strobes L.) stands. 2012 IEEE 4th International Symposium on Plant Growth Modeling, Simulation, Visualization and Applications, Shanghai, pp. 413-417, https://doi.org/10.1109/PMA.2012.6524866.

Wang, X.-P., Li, X.-R., Zhang, J.-G., Zhang, Z.-S., & Berndtsson, R. (2005). Measurement of rainfall interception by xerophytic shrubs in re-vegetated sand dunes. Hydrological Sciences Journal, 50(5), 897–910. https://doi.org/10.1623/hysj.2005.50.5.897

Watson, B. M., & Putz, G. (2014). Comparison of temperature-index snowmelt models for use within an operational water quality model. Journal of Environmental Quality, 43(1), 199–207. https://doi.org/10.2134/jeq2011.0369

Winchell, M., Srinivasan, R., Di Luzio, M., & Arnold, J. (2013). ArcSWAT Interface for SWAT 2012: User's Guide (p. 459). Texas AgriLife Research and USDA Agricultural Research Service; retrieved with ArcSWAT 2012 software on 09 Sep 2014 from https://swat.tamu.edu/software/arcswat/.

Yang, J., Reichert, P., Abbaspour, K. C., Xia, J., & Yang, H. (2008). Comparing uncertainty analysis techniques for a SWAT application to the Chaohe Basin in China. Journal of Hydrology, 358(1–2), 1–23. https://doi.org/10.1016/j.jhydrol.2008.05.012

Zhang, X., Srinivasan, R., Arnold, J., Izaurralde, R. C., & Bosch, D. (2011). Simultaneous calibration of surface flow and baseflow simulations: A revisit of the SWAT model calibration framework. Hydrological Processes, 25(14), 2313–2320. https://doi.org/10.1002/hyp.8058